Behaviour of turbulent transport in the vicinity of a magnetic island

E. Poli, A. Bottino, A. G. Peeters [‡]

Max-Planck-Institut für Plasmaphysik, Boltzmannstrasse 2

D-85748 Garching bei München, Germany

[‡] *Centre for Fusion, Space and Astrophysics, Department of Physics,*

University of Warwick, UK

Abstract

The influence of a static magnetic island on the behaviour of the electrostatic turbulence in a tokamak is investigated numerically employing global nonlinear gyrokinetic particle-in-cell simulations. The excitation of turbulence is modified by the magnetic topology of the island. Low mode numbers in the energy spectrum of the potential disturbances, corresponding to the island perturbation, are amplified by nonlinear coupling with the microinstabilities, particularly in the presence of strong turbulence. The associated large-scale flows affect the transport directly and through strain of small-scale eddies. The temperature profile determined numerically in the island region agrees qualitatively with analytic estimates; however, quantitative discrepancies are found.

I. INTRODUCTION

In the calculation of turbulent transport due to electrostatic or electromagnetic microinstabilities in tokamaks, the equilibrium configuration is usually supposed to be axisymmetric. However, large-scale magnetohydrodynamic instabilities like the tearing mode [1,2] , leading to the formation of helical structures (called magnetic islands) that destroy the toroidal symmetry of a tokamak, are often observed in fusion experiments. A saturated tearing mode can lead to a significant degradation of the energy confined in the plasma or even cause disruptive termination of a discharge. For these reasons, tearing modes are an area of very active research. In many tokamak reactors, the tearing mode is found to be driven unstable by the decrease of the bootstrap current due to the flattening of the pressure profile inside the island [3–5] (in this case, the mode is called Neoclassical Tearing Mode, NTM).

It is easy to imagine that the change in the magnetic topology due to the presence of a large helical perturbation influences the dynamics of transport. First of all, since a magnetic island reconnects the magnetic field on both sides of the rational surface where it develops, it provides a radial magnetic-field component, thus leading to the appearence of a huge radial *parallel* transport, which is otherwise absent in a tokamak. This is the origin of the flattening of the pressure profile within the reconnected region mentioned above. As the microinstabilities that lead to turbulence are driven by density and temperature gradients, this flattening drastically reduces the turbulence level in the island. Finally, the development and the shape of the turbulent structures can be modified by the helical magnetic field of the mode and by the interaction with the sheared flows connected to the large-scale (island) components of the electric field. On the other hand, the turbulence itself affects the dynamics of magnetic islands. First of all, small-scale electromagnetic fluctuations modify the seeding and growth processes [6–8] . Moreover, the competition between perpendicular and parallel transport contributes to determining the pressure profile around the island separatrix [9,10] , in a region which can be as large as the island itself in the early stage of the island evolution. The shape of the pressure profile has a strong impact on the island stability, first of all because it determines the level of the bootstrap current (and hence its neoclasical stability [9]), but also because the island rotation due to diamagnetic effects gives rise to a polarization current [11−13] which is found to be potentially important for the dynamics of small islands. The behaviour of the island propagation velocity in the presence of turbulence has been investigated recently employing a Hasegawa-Wakatani model in a slab configuration [14] .

A complete kinetic self-consistent solution of the problem of the island evolution in the presence of turbulence in a realistic tokamak geometry, which involves the resolution of time scales ranging from those typical of the particle orbits to those characterizing the island growth, is computationally prohibitive. The size of the problem can be reduced, e. g., by choosing a fluid approach to the computation of the turbulent fields, by simplifying the magnetic geometry (slab or cylindrical instead of toroidal), or by considering only short (turbulence-related) or long (island-related) time scales. A "minimal model" for a self-consistent description of turbulence and island dynamics has been put forward in Ref. [15] , which includes also a detailed discussion of the basic features of the mutual interaction between small-scale and large-scale instabilities typical of this problem.

In this paper, full toroidal geometry and a kinetic description of the ion behaviour are retained. Toroidicity and kinetic effects are known to play a fundamental role in the dynamics of both the turbulence and the tearing mode. On the other hand, in the model adopted here, the magnetic island is treated as a prescribed static perturbation of the background axisymmetric configuration, and its time evolution is disregarded. A particle-in-cell (PIC) approach is well suited for a direct numerical implementation of this model, since PIC codes are based on the integration of the trajectories of an ensemble of markers evolving according to a set of Hamiltonian equations of motion, where the magnetic-field perturbation due to the island can be included in a quite straightforward way. The self-consistent electric field is calculated by solving the Poisson equation on a fixed spatial grid. In the simulations presented here, performed employing the global gyrokinetic PIC code ORB5 [16,17] , only electrostatic microinstabilities are considered. With respect to the considerations made above, the model adopted here is used to describe the influence of the island on the development of the turbulence (spectrum, coupling to long-wavelengths modes, shape of the eddies etc.), to determine self-consistently the heat transport and its dependence on the island size and geometry and (related to this) to check the assumptions of previous studies on the transport properties in the island region.

It is noted in passing that a gyrokinetic approach is needed not only to properly treat the dynamics of the microinstabilities, but also because finite-orbit effects can become essential for small islands and in any case around the separatrix [18,19] .

In this paper, Sec. II is devoted to a description of the approach used to include an island structure in numerical simulations based on the PIC method. Some earlier results on the determination of the balance between perpendicular and parallel transport across a magnetic island are summarized in Sec. III. The numerical results of the ORB5 simulations are presented in Sec. IV. Some concluding remarks follow in Sec. V.

II. NUMERICAL SCHEME

A. The particle-in-cell code ORB5

The particle-in-cell method is based on the introduction of an ensemble of "super-particles", or markers, each one describing a piece of the phase space associated with a given particle species. The evolution of the markers is determined by the corresponding equations of motion, which are coupled to Maxwell's equations. The self-consistent fields are calculated projecting the charge and current associated with each marker onto a fixed spatial grid. This approach is implemented in the global gyrokinetic PIC code ORB5, which provides a numerical solution to the electrostatic approximation of the gyrokinetic equations in the formulation of T. S. Hahm [20] . The distribution function is split into an analytically-known time-independent part f_0 and a perturbation δf which is represented numerically. The gyrokinetic equations of motion for the markers are

$$\frac{\mathrm{d}\mathbf{R}}{\mathrm{d}t} = v_\parallel \mathbf{b} + \frac{1}{B_\parallel^*}\left[\frac{\mu B + v_\parallel^2}{\Omega_{ci}}\mathbf{b}\times\nabla B + \right.$$

$$\left. - \frac{v_\parallel^2}{\Omega_{ci}}\mathbf{b}\times(\mathbf{b}\times\nabla\times\mathbf{B}) - \nabla\langle\phi\rangle_g \times \mathbf{b}\,\right], \tag{1}$$

$$\frac{\mathrm{d}v_\parallel}{\mathrm{d}t} = -\mu\left[\mathbf{b} - \frac{v_\parallel}{B_\parallel^*\Omega_{ci}}\mathbf{b}\times(\mathbf{b}\times\nabla\times\mathbf{B})\right]\cdot\nabla B \tag{2}$$

$$- \frac{q_i}{m_i}\left\{\mathbf{b} + \frac{v_\parallel}{B_\parallel^*\Omega_{ci}}\left[\mathbf{b}\times\nabla B - \mathbf{b}\times(\mathbf{b}\times\nabla\times\mathbf{B})\right]\right\}\cdot\nabla\langle\phi\rangle_g,$$

$$\frac{\mathrm{d}\mu}{\mathrm{d}t} = 0, \tag{3}$$

where $\mathbf{R}$ is the position of the gyrocentre, $v_\parallel$ the velocity component along the magnetic field, $\mathbf{b}$ the unit vector along the magnetic field $\mathbf{B}$, μ the magnetic moment, Ω_{ci} the cyclotron frequency, $\langle\phi\rangle_g$ the perturbed potential (solution of the Poisson equation) averaged over the gyroperiod, q_i and m_i the particle's charge and mass, respectively, and $B_\parallel^* = B + (m_i/q_i)v_\parallel \mathbf{b}\cdot\nabla\times\mathbf{b}$. Since along the orbits $\mathrm{d}f/\mathrm{d}t = 0$, δf must obey the equation

$$\frac{\mathrm{d}(\delta f)}{\mathrm{d}t} = -\frac{\mathrm{d}f_0}{\mathrm{d}t} = -\mathbf{v}\cdot\nabla f_0 - \dot{v}_\parallel \frac{\partial f_0}{\partial v_\parallel}. \tag{4}$$

The δf method described above can be successfully applied to represent the deviation of the moments of the distribution function from the "unperturbed" state (when no island is present), as has been shown previously for the case of drift kinetic simulations [21,22].

The perturbed potential is obtained as the solution of the Poisson equation

$$\nabla^2\phi = 4\pi q_i\left\{n_e - \int\left[f + \frac{q_i}{m_i B}(\phi - \langle\phi\rangle)\frac{\partial f}{\partial\mu}\right]\delta(\mathbf{R}+\rho-\mathbf{r})\mathrm{d}^6\mathbf{Z}\right\}, \tag{5}$$

where ρ is a vector directed from the gyrocentre to the position of the particle and $\langle\phi\rangle$ is the flux-surface-averaged potential. The charge connected to each marker is assigned pointwise to a spatial mesh in order to provide the source term. The computation of the gyroaveraged density follows an adaptive procedure, in order to have the same number of sampling points per arclength along the gyro-ring. Once the perturbed gyroaveraged charge density associated with each marker has been projected onto the (B-spline) basis, the equation for the components of the potential on this basis reduces to an algebraic matrix equation. The same B-spline basis can be used to interpolate the radial magnetic-field perturbation associated with the magnetic island, which is initially assigned on a grid.

B. Including a magnetic island

In the presence of a (static) magnetic island, the tokamak magnetic field can be represented as

$$\mathbf{B} = \nabla\psi_t \times \nabla\xi/m + \nabla\varphi \times \nabla\Psi_{he}, \tag{6}$$

where ψ_t is the toroidal flux, $\xi = m\theta - n\varphi$ is the helical angle (θ and φ being the poloidal and toroidal angles, respectively, and m and n the poloidal and toroidal mode number associated to the island) and

$$\Psi_{he} = \psi - \frac{\psi_t}{q_s} + \alpha\cos\xi \tag{7}$$

is the helical flux (ψ is the poloidal flux and the subscript s denotes that a quantity is calculated at the resonant (m,n) surface), which can be used to label the perturbed magnetic surfaces, since $\mathbf{B}\cdot\nabla\Psi_{he} = 0$. In the limit of vanishing magnetic perturbation, $\alpha \to 0$, it is easy to show that Eqs. (6,7) reduce to the usual representation of the axisymmetric tokamak field. The last term of Eq. (7) describes the island magnetic field, which is therefore

$$\tilde{\mathbf{B}} = \alpha\nabla\varphi \times \nabla\cos\xi = m\alpha\sin\xi\nabla\theta \times \nabla\varphi$$

where the perturbation strength α is approximated to be a constant. With this assumption, the island field is directed along $\nabla\psi$. This radial component accounts for the most important modification of particle orbits [23] and has been included in ORB5 by operating the substitution $\mathbf{b} \to \mathbf{b} + \tilde{\mathbf{b}}$ (where $\tilde{\mathbf{b}} = \tilde{\mathbf{B}}/B$) in the first term of both Eq. (1) and Eq. (2).

Fig. 1a is a Poincaré puncture plot produced by following the orbits of 23 particles along the torus, the electrostatic potential being switched off. The dots obtained as the intersection of the trajectories with the plane $\varphi = 0$ show the pattern of the perturbed field lines, which coincides with the contour levels of Ψ_{he} (for this plot, particles with low energy and $v_{\|}/v \simeq 1$ have been employed to reduce their drift with respect to the flux surfaces). The density profile, obtained again in the absence of the electrostatic potential, is reported in Fig. 1b. Here and in the following, the flux-surface averages are performed in helical cells delimited by neighbouring surfaces of constant Ψ_{he}, according to the definition

$$\langle A \rangle = \lim_{\delta\Psi_{he}\to 0} \frac{\int_{\Psi_{he}-\delta\Psi_{he}}^{\Psi_{he}+\delta\Psi_{he}} A \, \mathrm{d}^3\mathbf{r}}{\int_{\Psi_{he}-\delta\Psi_{he}}^{\Psi_{he}+\delta\Psi_{he}} \mathrm{d}^3\mathbf{r}}. \tag{8}$$

The density profile shown in Fig.1b exhibits a clear flattening within the island. The contribution of the simulation markers, namely $\delta n = \int \mathrm{d}\Omega_p \delta f / V$ (where $\mathrm{d}\Omega_p$ is the phase-space element and V is the volume of the cell) is shown by the dashed line.

In the determination of the balance between parallel and perpendicular transport in the island region, an important role is played by the (θ -averaged) parallel gradient operator $\nabla_{\|} = \mathbf{b}\cdot\nabla = k_{\|}\, \partial/\partial\xi|_{\Psi_{he}}$. The parallel wavevector $k_{\|}$ defined through this expression for $\nabla_{\|}$ is proportional to the distance from the rational surface and to the magnetic shear:

$$k_{\|} = -\frac{m}{qR}\frac{\psi-\psi_s}{q_s}\frac{\mathrm{d}q}{\mathrm{d}\psi} = \frac{\epsilon_s s_s n}{r_s^2}\,(r-r_s), \tag{9}$$

where the first expression refers to a full toroidal geometry and the second to a slab or cylindrical geometry. In Eq. (9), ϵ is the inverse aspect ratio and $s = (r/q)\, \mathrm{d}q/\mathrm{d}r$ the magnetic shear.

III. PARALLEL AND PERPENDICULAR TRANSPORT CLOSE TO THE ISLAND SEPARATRIX

In the presence of a magnetic island, since the transport along the field lines is much larger than across the field, the pressure profile can be thought to be a function of the perturbed magnetic-flux label Ψ_{he} introduced above. Under this assumption, the pressure gradient jumps from a finite value to zero when the island separatrix is crossed. However, the ratio between, say, the parallel and perpendicular heat conductivity in a tokamak is indeed very large (up to $\chi_{\|}/\chi_{\perp} \approx 10^9 - 10^{10}$) but finite. As a consequence, a boundary layer appears around the island separatrix, along which the heat is transported from one side of the rational surface to the other [9,10]. The features of this process have been investigated solving the steady-state heat diffusion equation [9]

$$\chi_{\|}\nabla_{\|}^2 T + \chi_{\perp}\nabla_{\perp}^2 T = 0, \tag{10}$$

or, alternatively,[1] the kinetic equation [10]

$$v_{\|}\nabla_{\|} f = D_{\perp}\nabla^2 f. \tag{11}$$

The critical width w_c in which parallel and perendicular transport compete is obtained by equating the two terms of the previous equations. Thus in Eq. (10) one can estimate $\chi_{\|}k_{\|}^2 \sim \chi_{\perp}/w_c^2$, and assuming $r - r_s \sim w_c$ in Eq. (9), the scaling for w_c turns out to be $w_c/r \sim (\chi_{\perp}/\chi_{\|})^{1/4}(1/\epsilon_s s_s n)^{1/2}$. The corresponding estimate derived from Eq. (11), namely $w_c \sim (D_{\perp}/k_{\|}v_{\rm th})^{1/2}$, is reduced to the above if a parallel diffivity $D_{\|} \sim v_{\rm th}/k_{\|}$ is introduced (see footnote) and again taking $r - r_s \sim w_c$ in Eq. (9). In the transition layer, the temperature is not a flux-surface function. The heat is found to be transported along the layer and to flow across the rational surface near the X-point [9]. The analysis of Hazeltine *et al.* [10], moreover, predicts that the jump Δf of the distribution function on both sides of the island should be proportional to the gradient $\mathrm{d}f/\mathrm{d}r$ at the island separatrix, the proportionality factor being approximately given by the width of the critical layer $w_c \simeq \sqrt{\chi_{\perp}/k_{\|}v_{\rm th}}$. It has to be stressed that, in both approaches, the dependence of the perpendicular (heat) diffusion coefficient on the radial coordinate ψ and on the helical angle along the island ξ has been neglected, in order to obtain an analytic solution of the starting equation. In the next section, this picture is compared with the results of direct numerical simulations of turbulent transport.

---

[1]It is noted that replacing conduction by convection, i. e. replacing in Eq. (10) the term $\chi_{\|}\nabla_{\|}^2 T$ with $v_{\|}\nabla_{\|}T$ (which is in turn equivalent to estimating [9] $\chi_{\|} \sim v_{\rm th}/k_{\|}$) one obtains an equation of the same form as Eq. (11).

IV. NUMERICAL RESULTS

The numerical simulations presented in this section have been performed for a tokamak with circular concentric flux surfaces, major radius $R_0 = 3.3$ m and minor radius $a = 0.47$ m. A flat density profile is considered, the turbulent transport being caused by an electrostatic Ion-Temperature-Gradient (ITG) instability. As explained in Sec. II B, flux-surface ("zonal") averages have to be performed between surfaces of constant Ψ_{he}, which are not axisymmetric ($n = 0$) if a magnetic island is present. However, the assumption that the zonal potential coincides with an $n = 0$ mode is hard-wired in ORB5 when adiabatic electrons are considered. Therefore, within the adiabatic approximation, a proper computation of the zonal flows turns out to be extremly difficult and is excluded from the simulations presented here (i. e., $n = 0$ modes are set to zero). No source terms have been used, so that the temperature profile relaxes according to the level of the heat flux. In simulations of this kind, if the normalized gyroradius $\rho_* \equiv \rho_s/a$ is sufficiently small, the time evolution of both the temperature and heat flux profiles is slow, so that a "quasi-steady" state can be identified [24]. This approach has been used in most of global turbulence analysis and has been chosen as a standard benchmark case for European global codes [25]. For simulations without zonal flows like those described in this paper, a quasi-steady stated can be reached for $\rho_* < 1/200$ [see e. g. Ref. [17]]. In the ORB5 runs analyzed here, $\rho_* = 1/320$. As this corresponds to a pretty low value for the ion temperature, the ion streaming along the island is not very fast. Typical values of $\chi_{||}/\chi_\perp$ are therefore[2] in the range $10^6 - 10^7$.

An example of the evolution of the ion temperature profile in a typical ORB5 simulation is shown in Fig. 2. Since the temperature is initialized as a function of the unperturbed flux coordinate ψ, each run is started with a turbulence-free phase, in which only potential perturbations with low mode numbers are allowed. During this time, the ion temperature

---

[2]Here, according to Ref. [9], we estimate $\chi_{||} \sim v_{\rm th}/k_{||}$, see Sec. III

becomes constant on the perturbed (constant- Ψ_{he}) flux surfaces and flattens inside the island. Outside the island, the temperature gradient increases because the flux surfaces are on averaged "compressed" with respect to the unperturbed magnetic equilibrium. After this phase, turbulent modes are switched on. Under the influence of the turbulent transport, the temperature gradient outside the island decreases, at a particularly fast rate at the end of the linear phase (overshoot). At the end of the run, a phase with almost constant temperature gradients in the island region is observed. It is noted that the gradients are computed in this figure as the variation of the temperature with respect to the flux-surface averaged value of the radial coordinate, i. e. with respect to $\langle\psi\rangle$. In the calculation of heat conductivity (defined as ratio of heat fluxes and temperature gradients) presented below, the gradients are evaluated taking into account that the distance between neighbouring flux surfaces is a function of the helical angle ξ . Fig. 2b shows the flattened temperature profile at the end of the turbulence-free phase as a function of the radial (x -axis) and helical (y -axis) coordinates (the inner and outer separatrices are represented by the two vertical thick solid lines). For plotting reasons, the island is "stretched" along the x -axis at the X -points ($\xi = \mp\pi$). The resulting unphysical cells are displayed in white.

The first set of results presented here concerns the development of the turbulence in the presence of a magnetic island. In Fig. 3, the time evolution of the toroidal energy spectrum (averaged over the minor radius) is shown for two different values of the island width. Moving from the linear to the nonlinear phase the spectrum exhibits an inverse cascade to smaller mode numbers, as usually seen also when the island is absent. The nonlinear coupling between the "turbulent" modes (high n) and the "island" modes (low n) deserves particular attention. In these simulations with a (3,2) island, a coupling between mode numbers n_1 and n_2 in the turbulence spectrum satisfying the relation $n_1 = n_2 + 2$ is found in both the linear and nonlinear phase. The low- n modes amplification through this coupling with the small-scale turbulence is more evident when the island is larger. Moreover, the whole spectrum shifts to lower n for larger islands. In the simulations presented here, "seed" $n = 2$ and $n = 4$ harmonics arise during the turbulence-free phase of the run described above; under realistic conditions, in general, the low-n potential associated to the island rotation with respect to the plasma can play a similar role and interact nonlinearly with the fluctuating field of the microinstabilities. These low-n field components affect the transport in the island region in a twofold way . First of all, they yield a direct transport signal, in particular where high-n modes have smaller amplitude, for instance inside the island (an example is shown in Fig. 4). While the direct contribution of the large-scale modes to the transport *across* the separatrix is negligible, they are essential for the residual transport level *inside* the island and finally for the shape of the temperature profile close to the resonant surface. As they are generated through non-linear coupling with the background turbulence, their importance is directly related to the strength of the small-scale modes, cf. the discussion after Eqs. (12,13) below. The second effect of low-n modes on the transport is that they generate sheared flows which strain the turbulent eddies, thus reducing the transport level. This process, which is closely analog to the familiar effect of zonal flows on drift-wave turbulence, is predicted theoretically (see e. g. Ref. [15]) and is nicely confirmed in our simulations.

We now turn to the analysis of the transport in the island region. In the simulations, the formation of elongated eddies across the X-point region is often observed. These eddies split when they drift inside the island, where the temperature gradient is much smaller (it is recalled that the island has a fixed position in these runs). In the region of the plasma corresponding to the island's O-point ($\xi \simeq 0$), a breaking of the eddies close to the (in particular inner) separatrix is observed. In this regard, an interesting observation is that low-n components in the local energy spectrum are usually observed to prevail on the inner side of the island, whereas they are less strong on the outer side. Correspondingly, the turbulent eddies are seen to be more pronounced on the outer side. This is a strong indication that the amplitude of the turbulent modes is regulated by the sheared flows associated with low-n fields. These qualitative observations are confirmed by the transport levels measured numerically. An example is shown in Fig. 5a. Outside the island, in the O-point region, the $\mathbf{E}\times\mathbf{B}$ transport is strong, consistently with the fact that the flux surfaces are closer to each other and the temperature gradient is therefore higher. However, close to the island separatrix, the largest heat fluxes are often found in the X-point region, whereas the transport around the O-point is reduced. These features are found in both the linear and nonlinear phase. The turbulent transport is of course very low in the island core. The behaviour of the heat flux as a function of the helical angle ξ cannot be explained simply in terms of the different "distance" of the flux surcaces at the O-point as compared to the X-point (i. e. in terms of different local gradients). This can be seen in Fig. 5b, which reports the values of the heat conductivity. It is noted, in addition, that the penetration (spreading) of the turbulent structures into the outer side of the island leads to high values of the conductivity (relatively high transport in a region of low gradient). The ratio of the heat flux at the separatrix through X-point (q_X) and through the O-point (q_O) is reported in Fig. 6 as a function of the initial inverse gradient length and of the island width. The behaviour of q_X/q_O shown in Fig. 6a is due to the fact that, below a given value of the ∇T at the island, the formation of elongated eddies through the X-point mentioned above is reduced. Moreover, at higher gradients, i. e. when the turbulence is stronger, the large-scale sheared flows become stronger as well. The connected straining of the eddies close to the island separatrix seems to be more effective in the O-point region than in the X-point region (this result could change in the presence of strong zonal flows). The dependence of the ratio q_X/q_O on the island width reported in Fig. 6b has been computed for very similar values of the temperature gradient outside the island. Correspondingly, the ratio between the energy of small-scale and large-scale modes is comparable. The assumption that the transport level is determined by the interaction between low-n and turbulent flows would then explain the weak dependence of q_X/q_O on the island width and be consistent with the results shown in Fig. 6a.

The analytic predictions on the shape of the temperature profile across the island mentioned in Sec. III [9,10] are finally checked against direct numerical simulations of turbulent transport. The basic picture, according to which the temperature profile must exhibit a transition layer across the island separatrix, where it is not a flux-surface function, is qualitatively confirmed. It is recalled that, in addition to the finite perpendicular transport, finite-orbit effects also play a role in smoothing the pressure profile across the separatrix [21,22]. In the simulations, the ratio between the radial $\mathbf{E} \times \mathbf{B}$ flux

$$q_E = \int \frac{mv^2}{2} \, v_E \, \delta f \, \mathrm{d}^3\mathbf{v} \tag{12}$$

and the radial component of the parallel flux along the perturbed field lines

$$q_{\parallel,r} = \int \frac{mv^2}{2} \, v_\parallel \tilde{b} \, \delta f \, \mathrm{d}^3\mathbf{v} \tag{13}$$

is calculated. As expected, inside the island separatrix there is a layer where these fluxes are of the same order. Depending on the strength of the turbulence, the ratio $q_E/q_{\parallel,r}$ can be above or below one (as mentioned at the beginning of this section, the parallel streaming is not very fast in these simulations). In the very centre of the island, this ratio can be one or two order of magnitude higher than at the separatrix, depending on the temperature gradients set in the simulations. In the island centre, the parallel transport becomes less and less effective, since $k_\parallel$ is proportional to the distance from the rational surface, whereas turbulent structures can in some case reach the O-point or be transported there by the diamagnetic rotation of the instability. Moreover, the excitation of low-n modes inside the island is much stronger if the level of the background turbulence is increased, as discussed above. A consequence of the fact that large eddies can develop across the X-point is that heat can be transported across the resonant rational surface without undergoing the process of crossing the separatrix at the O-point and being transported to the X-point, which usually considered as the standard process for the transport of heat from one side of the rational surface to the other [9]. The suggested proportionality between the jump ΔT of the temperature profile on both sides of the island and the gradient $\mathrm{d}T/\mathrm{d}r$ at the island separatrix [10] has been investigated through a scan in the background temperature gradient for two different sets of simulation parameters. The result of this scan, reported in Fig. 7, is that the product $w_c \, \mathrm{d}T/\mathrm{d}r$ increases faster than ΔT if the temperature gradient is increased, whereas their ratio is predicted to be constant, cf. Sec. III. One possible explanation for this result is that the assumption of uniform (both across and along the island) heat conductivity is too crude (it is in fact never verified in the simulations). Close to the island separatrix, $\chi_\perp$ displays a strong variation as a function of the radius and in particular of the helical angle, see Fig. 5b. Moreover, $\chi_{\perp,X}$ and $\chi_{\perp,O}$ vary differently depending on plasma parameters, particularly on the temperature gradient, as shown above. Whether a diffusive ansatz can be used at all to describe the transport across the island separatrix is an interesting issue which will be addressed in the future.

V. DISCUSSION AND CONCLUSIONS

The investigation of the interaction between magnetic island and electrostatic drift-wave turbulence in a tokamak plasma presented in this paper is based on the solution of the gyrokinetic equation in a toroidal geometry. Emphasis has been placed on the modelling of the turbulent processes in the presence of a static island. Global electrostatic simulations have been performed employing the PIC code ORB5. PIC codes allow an –at least conceptually– straightforward implementation of a magnetic island through a modification of the equations of motion which take into account the presence of a small radial component of the magnetic field. The development of the turbulence is modified by the MHD mode through the associated flattening of the temperature gradient and through the interaction between large-scale (island) flows and small-scale (turbulence) flows. These low- n flows act both radially, providing an own transport signal, and azimuthally, straining the small-scale eddies. Using the terminology of Ref. [15], the feedback of large scales on small scales occurs both in position space and in $\mathbf{k}$ space. The numerical results obtained in this paper confirm the importance of the complex dynamics outlined above. In particular, the inhomogeneous behaviour of the transport both across and along the island has been stressed. The validity of a transport model for the island based on the assumption of uniform heat conductivity has been questioned. More basic questions concerning the diffusive nature of the transport in the island region remain to be explored.

As discussed in the Introduction, in this paper we aim rather at an accurate description of small-scale instabilities (through a global toroidal gyrokinetic approach) than at the resolution of the time scales connected with the island evolution. In this sense, the choice of a non-rotating island is linked to the fact that the present numerical scheme does not include the physics required for a self-consistent determination of the island rotation, which is connected to the dissipative phenomena leading to an "out-of-phase" current in the island region [26]. Correspondingly, the electrostatic potential associated with the island rotation cannot be determined self-consistently, whereas it is determined from the Poisson equation for the turbulent fluctuations. Anyway, since the island rotation is supposed to occur in the range of the diamagnetic frequency, its interaction with the drift waves [18] is potentially an important element for the island stability; moreover, the rotation frequency itself is expected to by influenced by the radial profiles [14], as already noted in Sec. I. Similarly, an important role in the seeding and in the first phase of the island growth is played by small-scale electromagnetic fluctuations, which are not retained in the electrostatic version of ORB5 employed here. However, as far as the transport properties of the plasma in the island region are concerned, an electrostatic approach is sufficient to address the relevant features of the process studied here (energy transport generated by small-scale disturbancies, nonlinear mode coupling, interaction between large and small scales, inhomogeneity of the transport properties in the island region, etc.).

It is recalled that, in the simulations presented here, the electrons were assumed to be adiabatic. In ORB5, the adiabatic approximation is implemented under the assumption of unperturbed flux surfaces. For these reason, zonal flows were excluded from the computation, and the calculation of low- n fields was not exact, in particular for large islands. A way to overcome this problem, thus obtaining more realistic prediction of the transport level in the island region, is to employ kinetic electron, which have the correct response to the island topology. It is important to recall, however, that the physics of self-regulation of turbulent transport through sheared flows connected to large-scale components of the electrostatic potential is not entirely excluded from our simulations, since the low- n fields due to the presence of the island provide an effect similar to that of zonal flows, as mentioned above. In this respect, on the contrary, the neglect of zonal flows in our simulations allows us to discuss the role of low-n modes on their own. The investigation of the zonal-flows-physics in the presence of a magnetic island is planned for the near future. The accurate calculation of the transport levels is crucial to make more realistic predictions on the stability of small islands in the presence of significant perpendicular transport and will allow a more quantitative analysis of threshold models [9] based on the "critical width" $w_c \propto (\chi_\perp/\chi_\parallel)^{1/4}$ mentioned in Sec. III.

REFERENCES

[1] FURTH, H. P. et al., Physics of Fluids **6** (1963) 459.

[2] RUTHERFORD, P. H., Physics of Fluids **16** (1973) 1903.

[3] QU, W. X. et al., University of Wisconsin Plasma Report **UWPR 85-5** (1985).

[4] CARRERA, R. et al., Physics of Fluids **29** (1986) 899.

[5] CHANG, Z. et al., Physical Review Letters **74** (1995) 4663.

[6] ITOH, S.-I. et al., Plasma Physics and Controlled Fusion **46** (2004) 123.

[7] YAGI, M. et al., Nuclear Fusion **45** (2005) 900.

[8] ISHIZAWA, A. et al., Physics of Plasmas **14** (2007) 040702.

[9] FITZPATRICK, R., Physics of Plasmas **2** (1995) 825.

[10] HAZELTINE, R. D. et al., Physics of Plasmas **4** (1997) 2920.

[11] SMOLYAKOV, A. I. et al., Physics of Plasmas **2** (1995) 1581.

[12] WILSON, H. R. et al., Physics of Plasmas **3** (1996) 248.

[13] POLI, E. et al., Physical Review Letters **94** (2005) 205001.

[14] MILITELLO, F. et al., Physics of Plasmas **15** (2008) 050701.

[15] MCDEVITT, C. J. et al., Physics of Plasmas **13** (2006) 032302.

[16] JOLLIET, S. et al., Computer Physics Communications **177** (2007) 409.

[17] BOTTINO, A. et al., Physics of Plasmas **14** (2007) 010701.

[18] WAELBROECK, F. L. et al., Physical Review Letters **87** (2001) 215003.

[19] JAMES, M. et al., Plasma Physics and Controlled Fusion **48** (2006) 1647.

[20] HAHM, T. S., Physics of Fluids **31** (1988) 2670.

[21] POLI, E. et al., Physical Review Letters **88** (2002) 075001.

[22] POLI, E. et al., Plasma Physics and Controlled Fusion **45** (2003) 71.

[23] WHITE, R. B. et al., Physics of Fluids **26** (1983) 2958.

[24] SCOTT, B. D., Physics of Plasmas **12** (2005) 102307.

[25] FALCHETTO, G. L. et al., Plasma Physics and Controlled Fusion **50** (2008) 124015.

[26] SMOLYAKOV, A. I., Plasma Physics and Controlled Fusion **35** (1993) 657.

Figure captions

Fig. 1: ORB5 simulation performed excluding the self-consistent electric fields to highlight the motion of the ions along the perturbed field lines in the presence of a magnetic island: Poincaré puncture plot (a) and radial density profile (b).

Fig. 2: Time evolution of the temperature gradient in the island region in a typical ORB5 simulation (a). In the turbulence-free phase, the profile flattens in the centre of the island and peaks just outside because of the "compression" of the magnetic surfaces. In the turbulent phase, the profile relaxes to a lower value of the gradient. The time is expressed in units of a/c_s (where c_s is the sound speed). Temperature profile at the end of the turbulence-free phase (b) as a function of the radial coordinate $\langle\sqrt{\psi}\rangle$ and of the helical angle ξ (where $\xi = \mp\pi$ corresponds to the X-point, $\xi = 0$ to the O-point) for a large island ($W/a \simeq 0.1$).

Fig. 3: Time evolution of the energy spectrum of the turbulence for a large ($W/a \simeq 0.1$, a) and small ($W/a \simeq 0.04$, b) island, showing the coupling between large-scale and small-scale fields. The y-axis reports the logarithm of the toroidal-mode energy normalized to $m_i c_s^2$.

Fig. 4: $\mathbf{E} \times \mathbf{B}$ heat flux defined in Eq. (12) as a function of $\langle\sqrt{\psi}\rangle$ and of the helical angle ξ for a large island ($W/a \simeq 0.1$). The transport due to the large-scale field components (with different directions) is clearly visible inside the island.

Fig. 5: Heat flux (a) and heat conductivity (b) in the nonlinear phase, for a mid-size island ($W/a \simeq 0.06$).

Fig. 6: Dependence of the ratio between the heat flux across the inner island separatrix at $\xi = \pi$ (X-point region) and at $\xi = 0$ (O-point region) on the initial temperature gradient at constant island width (a) and on the island width at constant temperature gradient (calculated at the beginning of the turbulence phase) (b).

Fig. 7: Ratio between the "jump" of the ion temperature at the island separatrix and the

product of the critical layer w_c times the temperature gradient as a function of the initial temperature gradient.

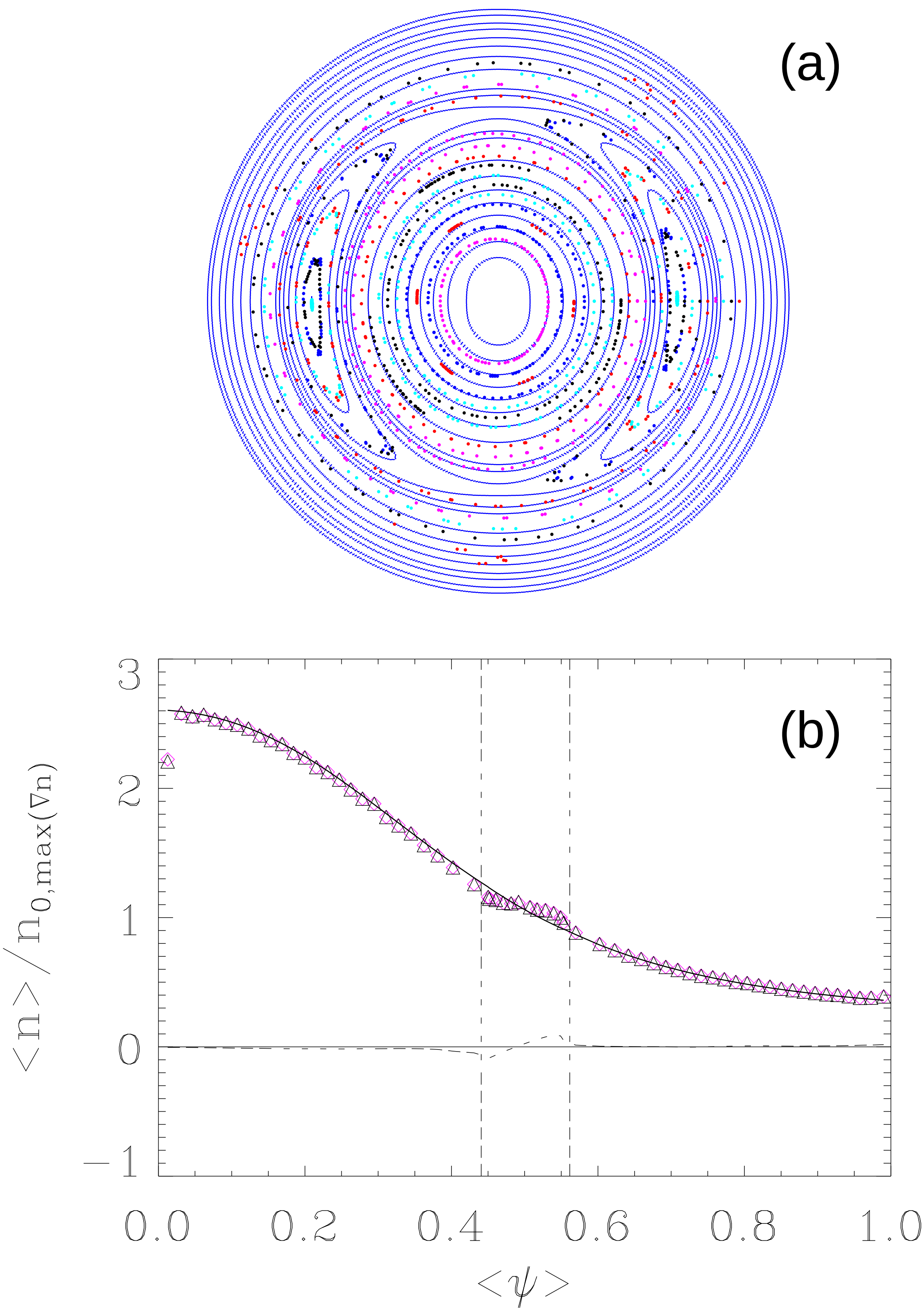

(a)
(b)
$\langle n \rangle / n_{0,\max(\nabla n)}$
$\langle \psi \rangle$
3
2
1
0
−1
0.0
0.2
0.4
0.6
0.8
1.0

(a)

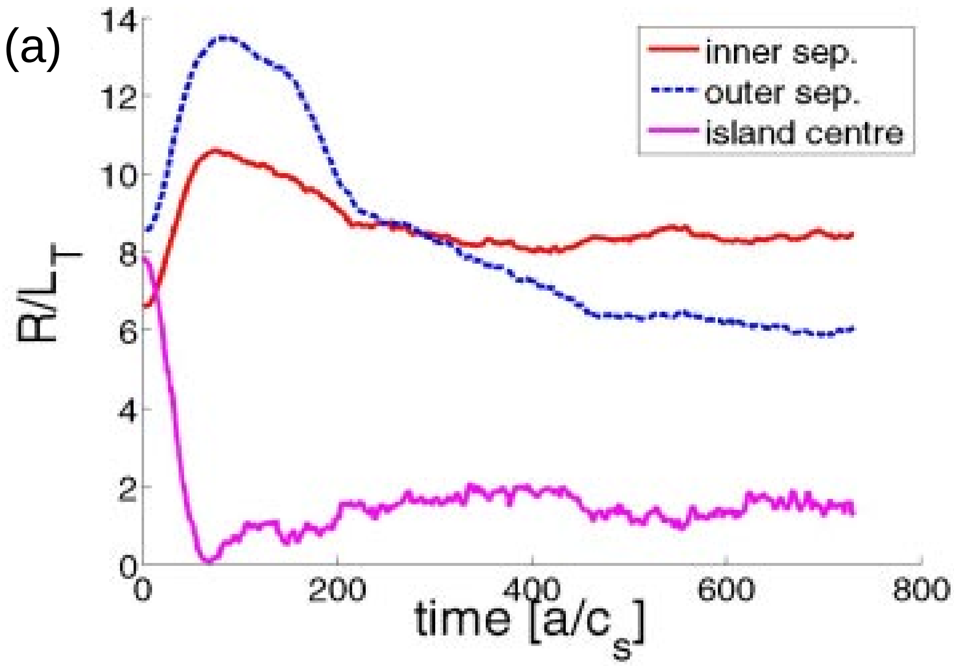
inner sep.
outer sep.
island centre
R/L_T
time [a/c_s]
0
2
4
6
8
10
12
14
200
400
600
800

(b)

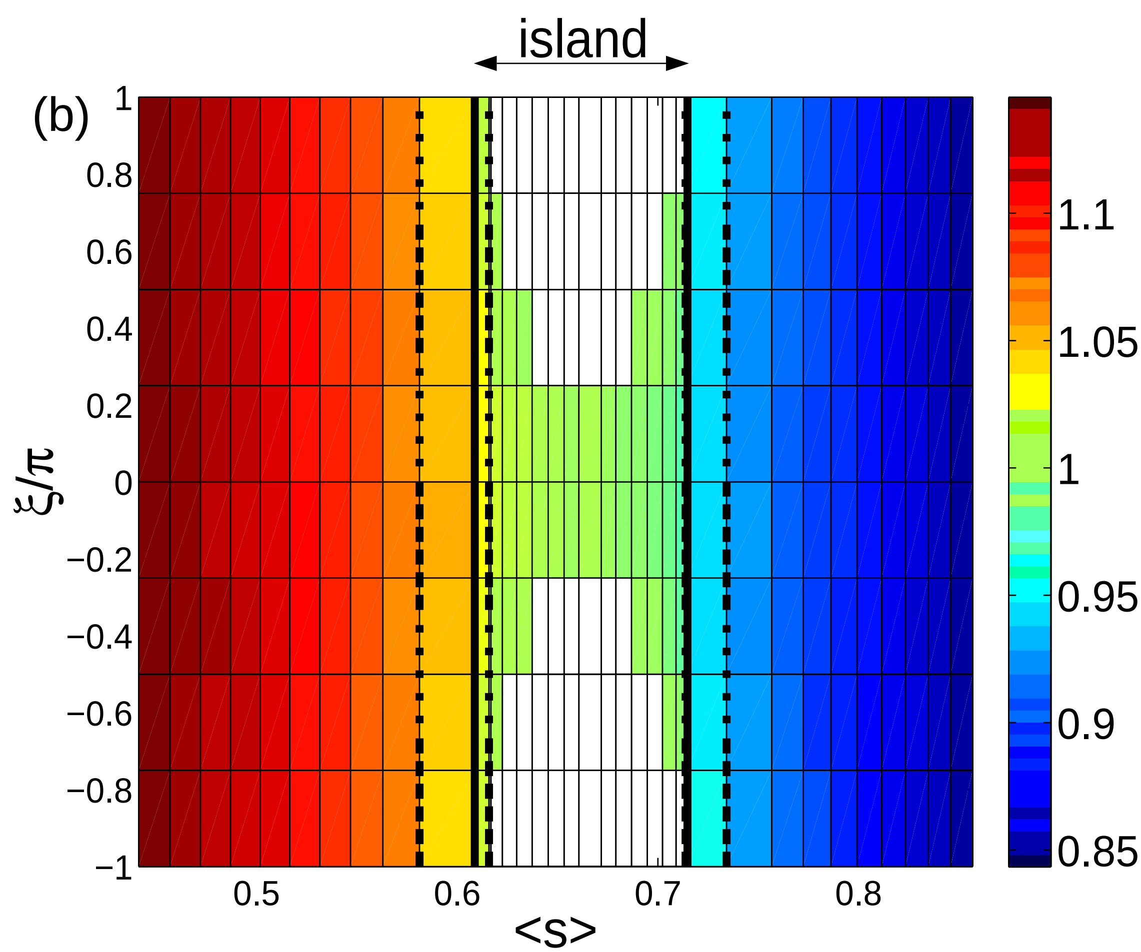
island
ξ/π
<s>
1
0.8
0.6
0.4
0.2
0
−0.2
−0.4
−0.6
−0.8
−1
0.5
0.6
0.7
0.8
1.1
1.05
1
0.95
0.9
0.85

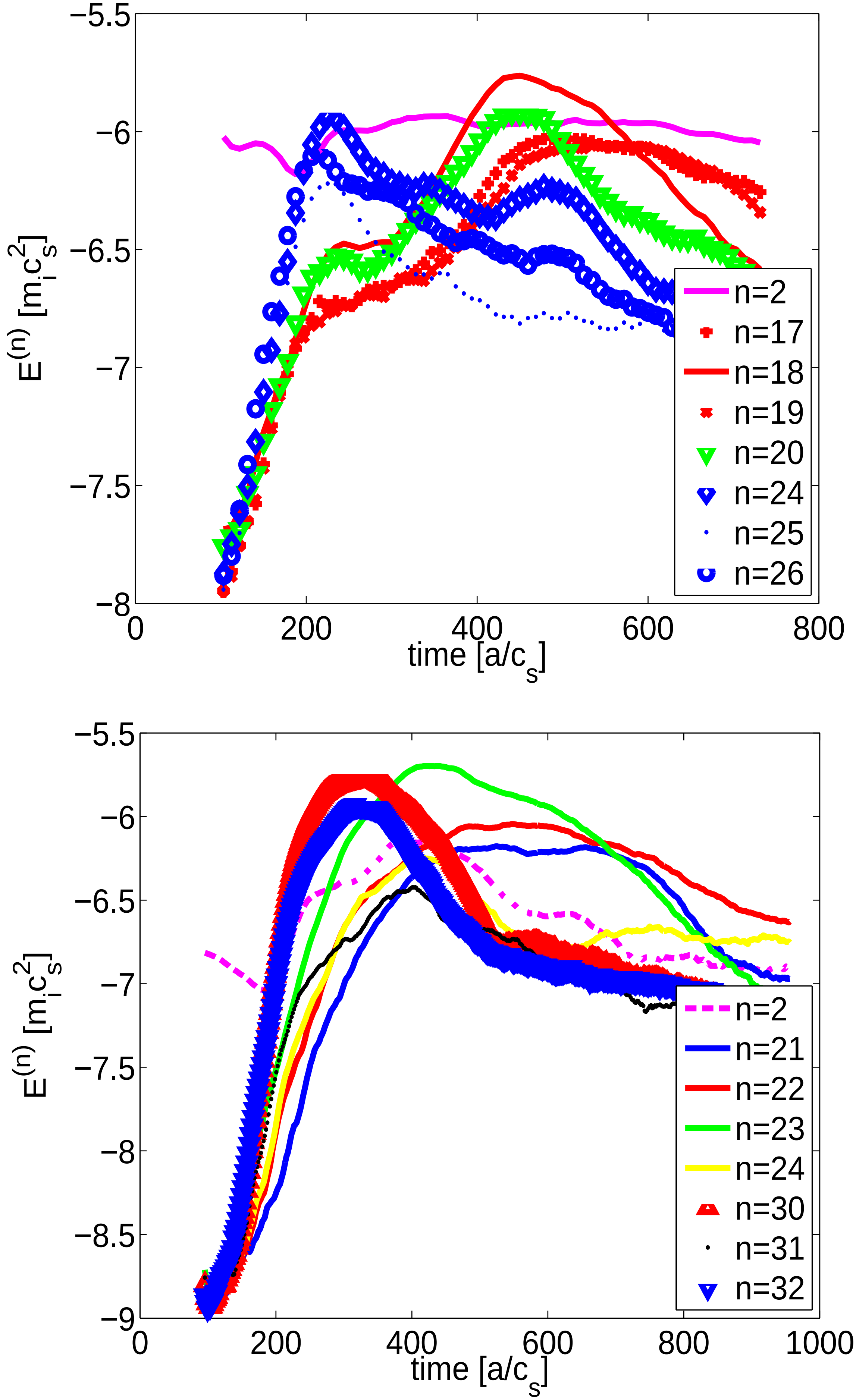

−5.5
−6
−6.5
−7
−7.5
−8
0
200
400
600
800
$E^{(n)}$ [$m_i c_s^2$]
time [a/c_s]
n=2
n=17
n=18
n=19
n=20
n=24
n=25
n=26
−5.5
−6
−6.5
−7
−7.5
−8
−8.5
−9
0
200
400
600
800
1000
$E^{(n)}$ [$m_i c_s^2$]
time [a/c_s]
n=2
n=21
n=22
n=23
n=24
n=30
n=31
n=32

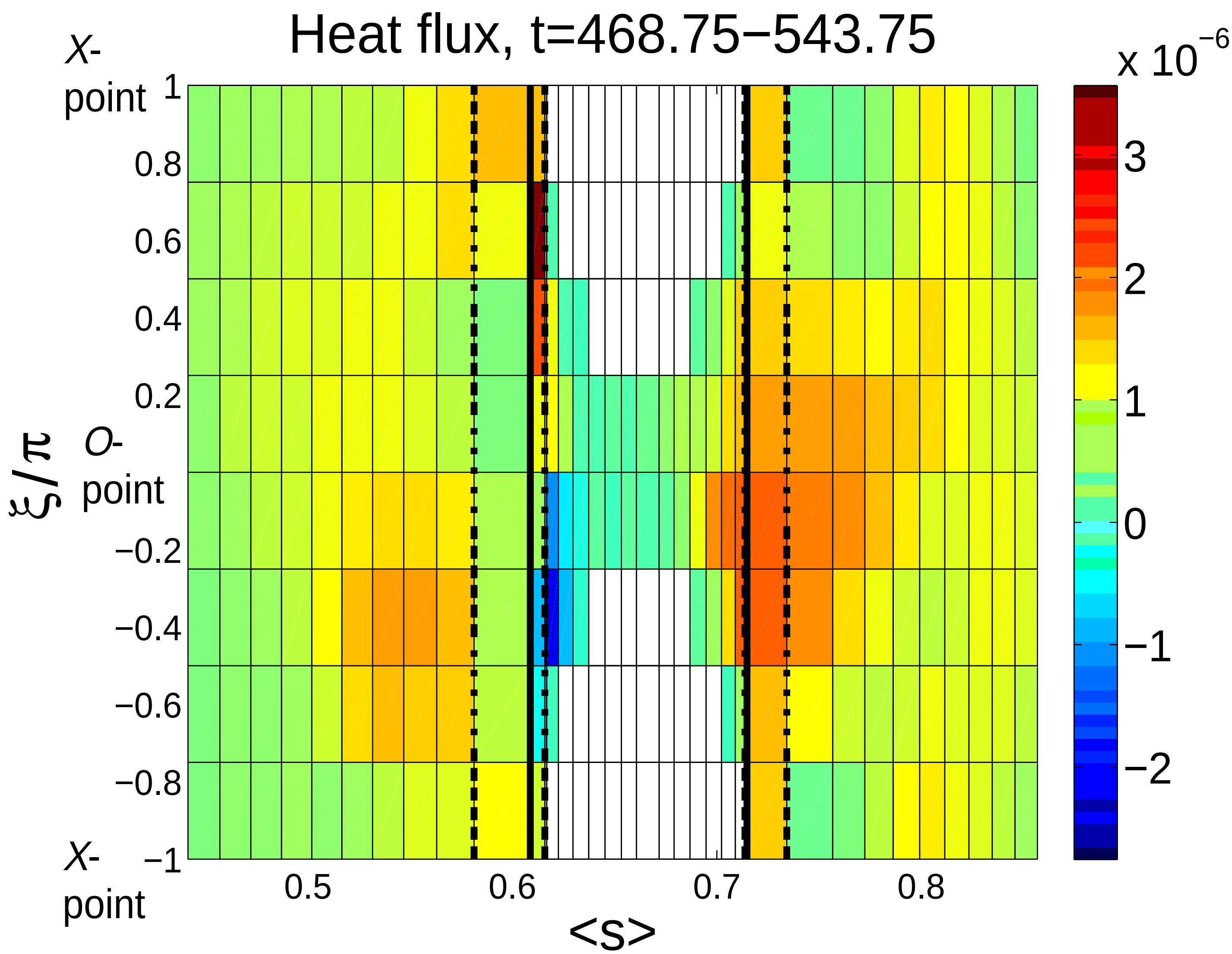
Heat flux, t=468.75−543.75
x 10^-6
X-point
O-point
X-point
ξ/π
<s>
1
0.8
0.6
0.4
0.2
−0.2
−0.4
−0.6
−0.8
−1
0.5
0.6
0.7
0.8
3
2
1
0
−1
−2

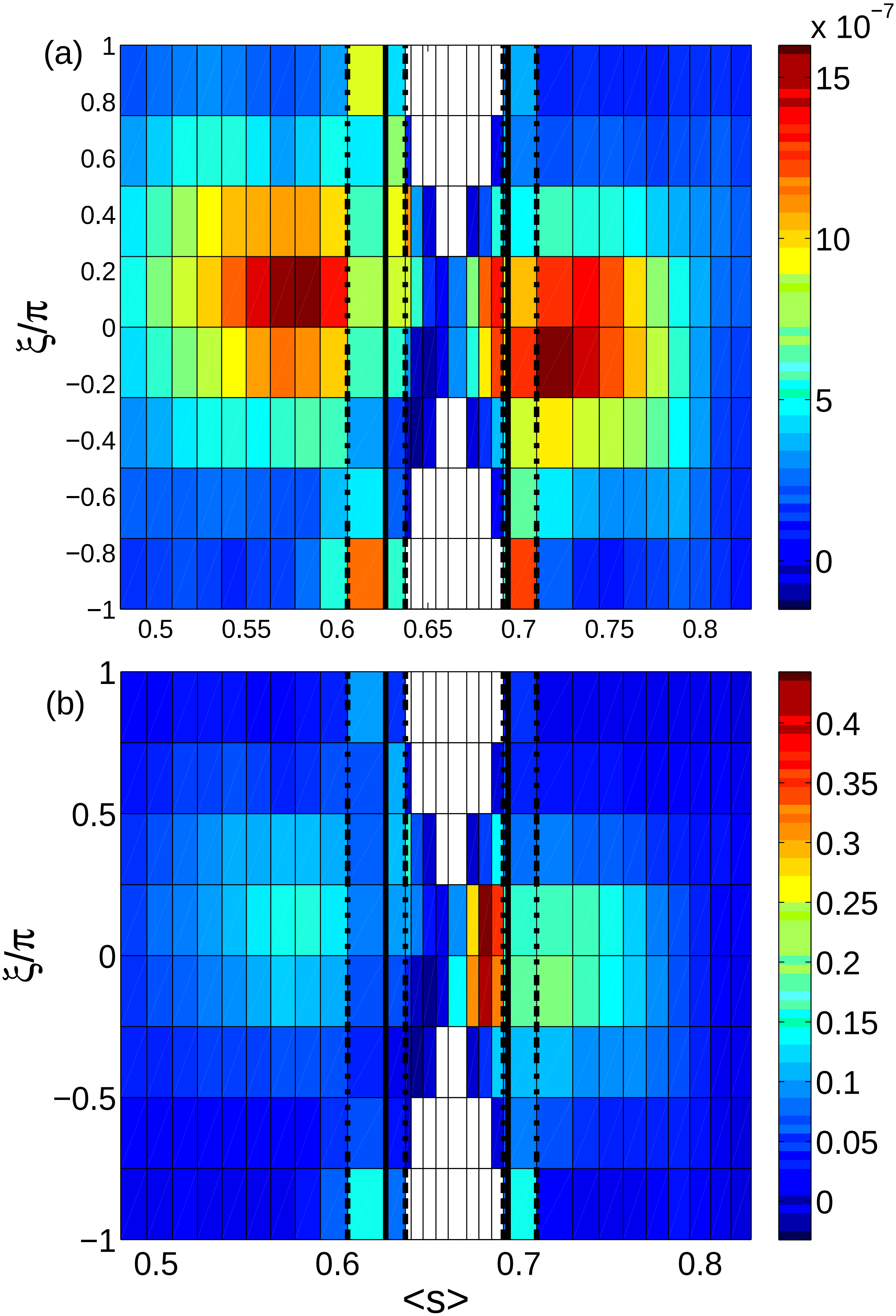

(a)
x 10^{-7}
15
10
5
0
ξ/π
1
0.8
0.6
0.4
0.2
0
−0.2
−0.4
−0.6
−0.8
−1
0.5
0.55
0.6
0.65
0.7
0.75
0.8
(b)
0.4
0.35
0.3
0.25
0.2
0.15
0.1
0.05
0
ξ/π
1
0.5
0
−0.5
−1
0.5
0.6
0.7
0.8
<s>

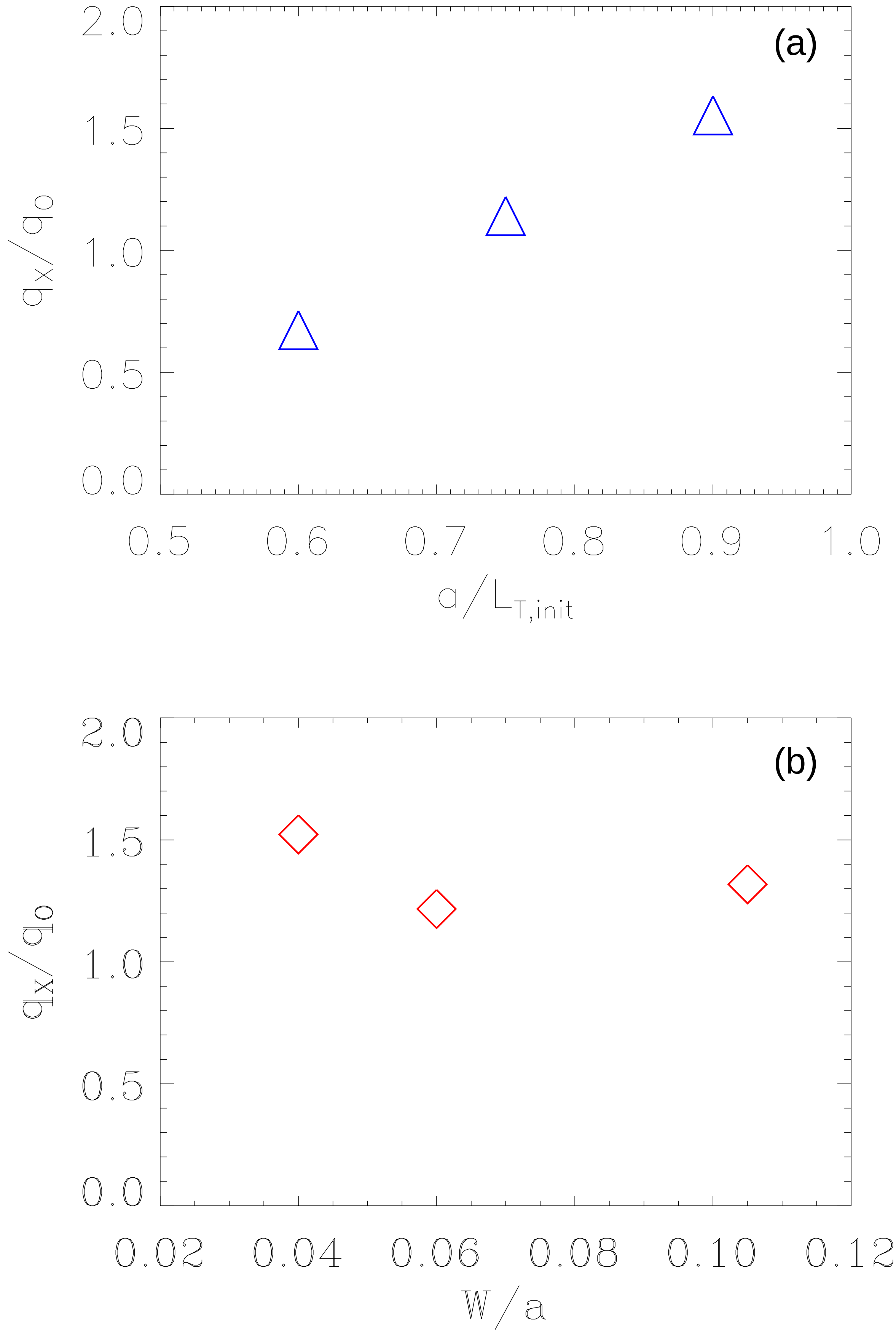

(a)
2.0
1.5
1.0
0.5
0.0
q_x/q_o
0.5
0.6
0.7
0.8
0.9
1.0
$a/L_{T,init}$
(b)
2.0
1.5
1.0
0.5
0.0
q_x/q_o
0.02
0.04
0.06
0.08
0.10
0.12
W/a

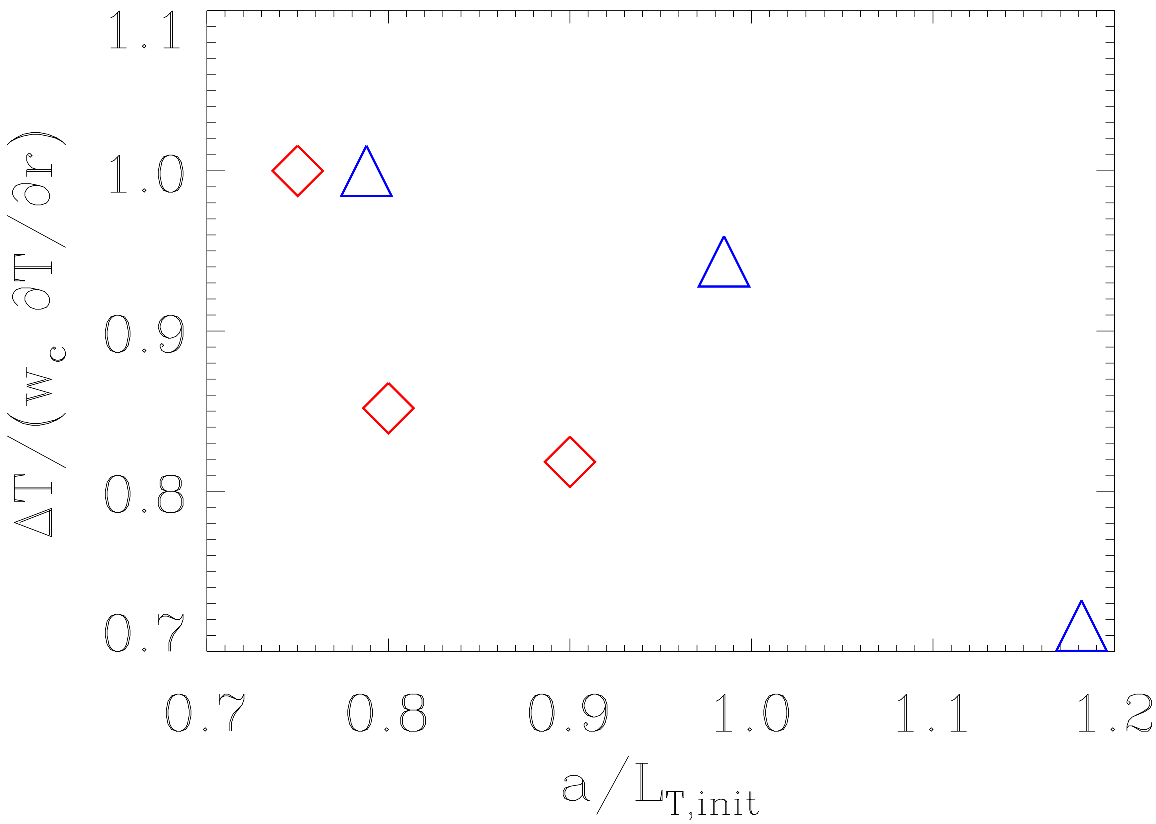

1.1
1.0
0.9
0.8
0.7
ΔT/(w_c ∂T/∂r)
0.7
0.8
0.9
1.0
1.1
1.2
a/L_T,init